Electrostatic Shield for Lunar Dust Entering Mechanical Seals of Lunar Exploration Equipment

Hiroyuki Kawamoto[1]

Abstract: A unique shield system for lunar dust has been developed using electrostatic force to prevent dust from entering into bearings and mechanical seals of equipment used for lunar exploration. A single-phase rectangular high voltage is applied to insulated parallel-plate electrodes printed on the edges of the gap in the mechanical sealing part. It was demonstrated that more than 70% of the dust was repelled from the gap with very little power, and it was predicted by numerical calculations performed using the distinct element method that the shielding performance of the system would improve further in the low-gravity and vacuum environment of the Moon. This technology is expected to increase the reliability of equipment used in long-term manned and unmanned activities on the lunar surface. **DOI: 10.1061/(ASCE)AS.1943-5525.0000272.**

Author keywords: Aerospace engineering; Dynamics; Particles; Electrical equipment; Soils; Space exploration.

Introduction

The lunar surface is covered by a regolith (soil) layer; approximately 20% of the volume of this material consists of particles less than 20 μm in diameter (McKay et al. 1991). Because of its small-sized particles and low lunar gravity, lunar dust can easily be lofted above the surface with any kind of disturbance. It has been known since the Apollo era that the dust on the Moon can cause serious problems for exploration activities [National Aeronautics and Space Administration (NASA) Manned Spacecraft Center 1970]. One of the major problems is that lofted dust enters into gaps of bearings and mechanical seals (Gaier 2005; Wagner 2006); such a situation could lead to catastrophic damage. To overcome this problem, a unique cleaning system has been developed using electrostatic force to remove lunar dust adhered to the surface of equipment used for lunar exploration (Calle et al. 2010; Kawamoto and Miwa 2011). A single-phase voltage is applied to parallel electrodes printed on a flexible substrate to remove the dust. This system is suitable for the dust removal from a flat part such as a door of a Pressurized Excursion Module; however, it cannot prevent dust from entering into the clearance such as bearings and mechanical seals of equipment. On the contrary, a mechanical seal is conventionally used for this purpose. Delgado and Handschuh (2010) demonstrated the performance of a spring-loaded Teflon seal in vacuum environment. It shows good sealing ability for rotating shafts; however, short lifetime and large braking torque are intrinsic issues of the mechanical seal. Suzuki et al. (2010) are developing a brush-type seal to mitigate these issues. It has been reported that the brush seal combined with a labyrinth seal has good sealing ability against dust simulant with low braking torque; however, some amount of dust accumulates between the brush and the labyrinth seal, particularly during the operation in vacuum. Therefore, a short lifetime is a cause of concern for this method.

This paper proposes a new shield system for lunar dust as an additional countermeasure to mitigate the load of the mechanical shield and thereby improve the overall performance of the mechanical equipment used for lunar exploration. The proposed system works on a simple principle. As shown in Fig. 1, a single-phase, rectangular high voltage was applied to the insulated parallel-plate electrodes pasted on the edges of the gap. Owing to the Coulomb force and dielectrophoresis force acting on the lofted particles, the particles are attracted to the electrodes along the electrical flux lines. Because application of a single-phase voltage does not generate a traveling wave (Kawamoto et al. 2006, 2011), particles are not transported in one direction; rather, they are repelled from the gap. An alternating electrostatic field acts as a barrier against dust on the basis of a principle similar to that of an electrostatic cleaning system developed for spacesuits (Kawamoto and Hara 2011) and mechanical parts (Kawamoto and Miwa 2011). This technology is expected to improve the reliability of equipment used for long-term manned and unmanned activities on the lunar surface.

System Configuration

Electrostatic Dust-Shielding Device

The dust-shielding device consists of aluminum parallel plate electrodes that are 35 mm long, 3 mm wide, and 0.2 mm thick. The surface of the electrodes was covered with insulating films made of polyimide (60 μm thick) to prevent insulation breakdown between the electrodes. The electrodes were pasted on the edges of the plastic plates (35 mm long and 2 mm thick) separated by a distance of 1 mm. It should be mentioned that a narrow gap is preferable for achieving a high shielding performance; however, a relatively wide gap of 1 mm was used in this experiment to demonstrate the effectiveness of the system. Use of narrow-gap configuration for a mechanical seal is expected to yield a performance higher than that achieved in this study.

Power Supply

This study used the power supply that was originally designed and used for the cleaning system of spacesuits (Kawamoto and Hara 2011) and mechanical parts (Kawamoto and Miwa 2011). A single-phase,

[1]Professor, Dept. of Applied Mechanics and Aerospace Engineering, Waseda Univ., Tokyo 169-8555, Japan. E-mail: kawa@waseda.jp

Note. This manuscript was submitted on May 11, 2012; approved on August 22, 2012; published online on August 30, 2012. Discussion period open until August 1, 2014; separate discussions must be submitted for individual papers. This paper is part of the ***Journal of Aerospace Engineering***, Vol. 27, No. 2, March 1, 2014. ©ASCE, ISSN 0893-1321/2014/2-354–358/$25.00.

rectangular high voltage, as shown in Fig. 1, was generated using a set of positive and negative amplifiers; the amplifiers were switched by semiconductor relays that were controlled by a microcomputer. The power supply is designed to be simple, compact, and lightweight for space applications.

Lunar Dust Simulant and Dust Feeder

The lunar dust simulant FJS-1 (Shimizu, Tokyo, Japan) (Kanamori et al. 1998), which is almost identical to the simulant JSC-1A (Orbital Technologies, Madison, Wisconsin), was used in the present experiments. Specifications of the particles are listed in Table 1, and their scanning electron microscope (SEM) images are shown in Fig. 2. The particle size distribution of FJS-1 is shown in Fig. 3 (Kawamoto et al. 2011; Kawamoto and Hara 2011).

To evaluate the system performance, dust must be fed continually at a constant rate. This condition was realized using a vibrating dust feeder. Lunar dust simulant was mounted on a sand sieve (106-μm opening) that was placed above the dust-shielding device; the sieve was then vibrated in the vertical direction using an electromagnetic shaker (Shinken, Tokyo, Japan, G14-818). The shielding device was isolated mechanically from the shaker. The feed rate of the dust was controlled by adjusting the magnitude and frequency of the excited mechanical vibrations. The attained repeatability of the feed rate was 7% (SD). This implies that the deduced shield rate contains at least 7% error.

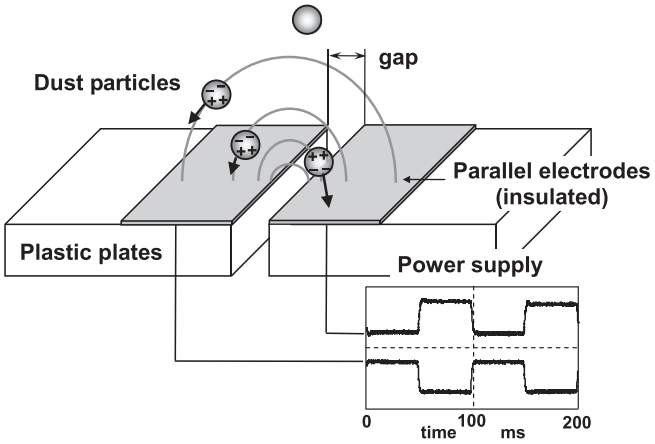

Fig. 1. Configuration and principle of electrostatic dust shield

Table 1. Properties of Lunar Soil Simulants FJS-1 and JSC-1A

Parameter	Specific gravity (g/cm)	Composition	Wt (%)
FJS-1	2.7	SiO_2	49.4
		TiO_2	1.6
		Al_2O_3	10
		Fe_2O_3	4.4
		FeO	8
		MgO	5.2
		CaO	9.3
		Na_2O	2.9 (alkalis)
JSC-1A	2.5	SiO_2	46–49
		TiO_2	1–2
		Al_2O_3	15.4–15.5
		Fe_2O_3	3–4
		FeO	7–7.5
		MgO	8.5–9.5
		CaO	10–11
		Na_2O	2.5–3

Shield Performance

Effect of Applied Voltage, Feed Rate, Frequency, and Device Configuration

The plot of the measured shield rate versus the applied voltage is shown in Fig. 4 using solid symbols and the solid curve. The experiments were conducted in air (20–25°C, 1 atm, 40–60 RH). The feed rate of dust normalized by the gap area (1×35 mm) was

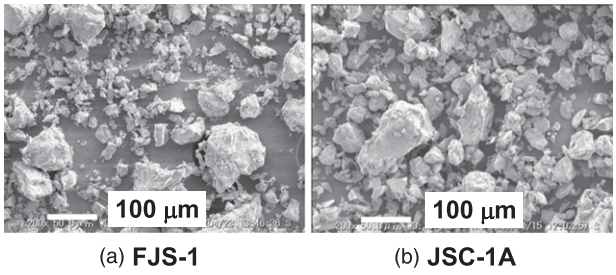

Fig. 2. SEM images of lunar soil simulants FJS-1 and JSC-1A: (a) FJS-1; (b) JSC-1A

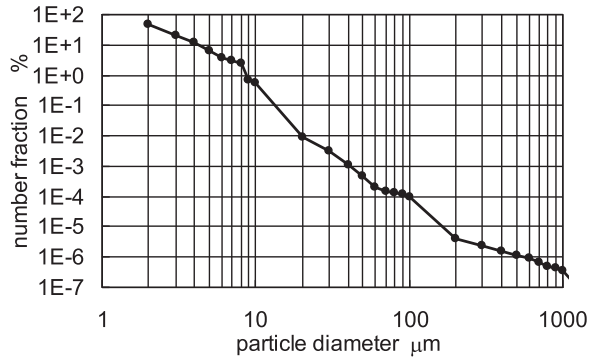

Fig. 3. Particle size distribution of lunar regolith simulant FJS-1

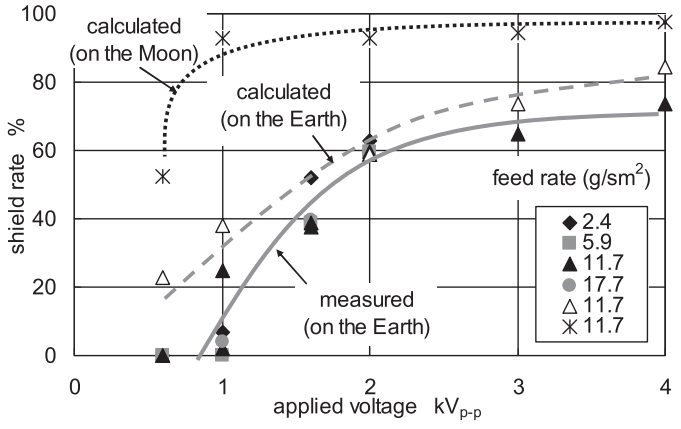

Fig. 4. Shield rate of the dust-shielding device versus applied voltage (frequency of applied voltage: 10 Hz)

J. Aerosp. Eng., 2014, 27(2): 354-358

selected as another parameter with respect to which the shielding performance was measured. The shield rate is determined as the weight of particles entering the gap under the applied voltage for 30 s divided by the weight of particles entering the gap in the absence of voltage. Dust was shielded above a threshold voltage of approximately 0.9 $kV_{p\text{-}p}$, and the shield rate increased with the applied voltage almost irrespective of the feed rate in the range of 2.4 to 17.7 g/sm^2. However, the improving shield performance reached saturation at voltage higher than 2 $kV_{p\text{-}p}$, and the shield performance was limited by the occurrence of the corona discharge in the air at voltage higher than 4.1 $kV_{p\text{-}p}$. The maximum shield rate was approximately 74% at the voltage just below that at which corona discharge began. The performance would improve further in vacuum because corona discharge does not occur in vacuum; therefore, the voltage limit can be increased.

The solid triangular marks in Fig. 5 show the experimentally measured shield rate at different frequencies of the applied voltage. The shield performance was high at low frequencies, and it was highest at 10 Hz. To investigate the dynamics of dust in the alternating electrostatic field, the motion of the particles was observed from the lateral side of the device using a high-speed microscope camera (Fastcam-max 120K model 1, Photoron, Tokyo, Japan). It was observed that the motion of dust synchronized the AC voltage at low frequency but it did not follow the change of polarity at high-frequency operation. It was confirmed from direct observation that the asynchronous motion of dust at high frequency caused a reduction of the shield performance. On the contrary, shielding is possible even when the frequency of the applied voltage is zero; however, under application of a DC voltage, the shielded dust accumulates on the electrodes, and it is not repelled from the surface of the electrodes. Therefore, application of low-frequency AC voltage is indispensable for a long-term operation.

To investigate the effect of the electrode configuration, additional experiments were conducted in cases that the electrode width was 1 mm and the electrodes were separated by a distance of 2 mm. The experimental results showed that the shield performance was almost independent of the electrode width and the gap between the electrodes at the threshold voltage because the applied voltage is limited by the occurrence of corona discharge. The corona onset voltage is determined by the electrostatic field. The effect of the inclination of the device was also investigated because the sealing part is not always in a horizontal position in actual operation. The shield rate when the plate was inclined 30° was about 70% of that at a horizontal position. It was observed using the high-speed microscope camera that some particles that fell on the upper plate rolled downward into the gap; this phenomenon caused a reduction of the shield rate. However, the weight of particles entering the gap when the plate was inclined is smaller than when the plate is horizontal because the horizontally projected area of the inclined gap is narrower than that of the horizontal gap for the vertically falling dust. Therefore, the horizontal position is the severest case.

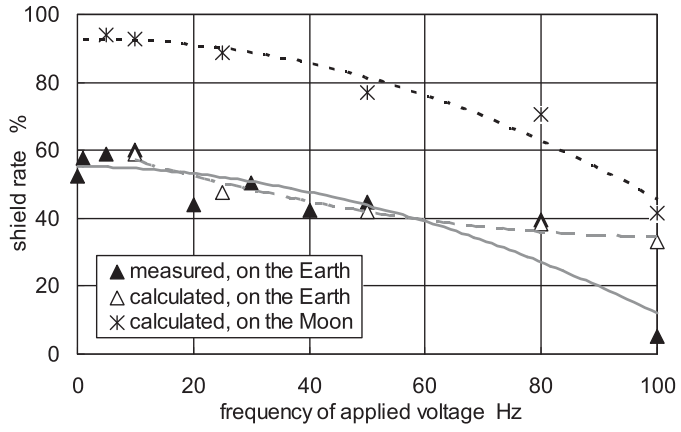

Fig. 5. Shield rate of the dust-shielding device versus frequency of applied voltage (dust feed rate: 11.7 g/sm^2, applied voltage: 2 $kV_{p\text{-}p}$)

Power Consumption

The power consumption of the dust-shielding device is shown in Fig. 6. The ordinate of the figure represents the power loss (input to the device) per unit length of the device under the assumption that the power loss is proportional to the length of the electrode. Because the transient current flowed immediately after the application of the voltage, the power loss is proportional to the frequency. On the other hand, power loss is proportional to the square of the applied voltage if insulation breakdown does not occur (Kawamoto et al. 2011). Because the voltage limit for insulation breakdown is 4 $kV_{p\text{-}p}$ and the optimal frequency is 10 Hz for the dust shield, the power consumption is only 7.3 mW for a 1-m-long device; the power consumption of this system is extremely low.

Observations and Calculation of Particle Motion

The numerical calculations were performed using a three-dimensional hard-sphere model using the distinct element method (Kawamoto et al. 2011). The basic equation of motion of a particle i of a system with six degrees of freedom is as follows:

$$m_i\ddot{\mathbf{x}}_i = -6\pi\eta R\dot{\mathbf{x}}_i + q_i\mathbf{E} + \mathbf{F}_{\text{image}} + \mathbf{F}_{\text{dipole}} + \mathbf{F}_{\text{adhesion}} + m_i\mathbf{g}, \quad I_i\ddot{\boldsymbol{\theta}}_i = 0, \tag{1}$$

where $\mathbf{x} = (x, y, z)$, $\boldsymbol{\theta} = (\theta_x, \theta_y, \theta_z)$; m = mass of the particle; η = viscosity of air; R = radius of the particle; q = charge of the particle; $\mathbf{E}$ = electrostatic field; $\mathbf{g}$ = gravitational acceleration; and I = inertia of the particle. Eq. (1) indicates that the particle motion is determined by the air drag, Coulomb force qE acting on a charged particle, electrostatic image force $\mathbf{F}_{\text{image}}$ on a charged particle over the electrodes, dielectrophoresis force $\mathbf{F}_{\text{dipole}}$ on a polarized particle in the nonuniform electrostatic field (Jones 1995), van der Waals adhesion force $\mathbf{F}_{\text{adhesion}}$ when the particle is in contact with the device and other particles, and the gravitational force $m\mathbf{g}$. The electric field

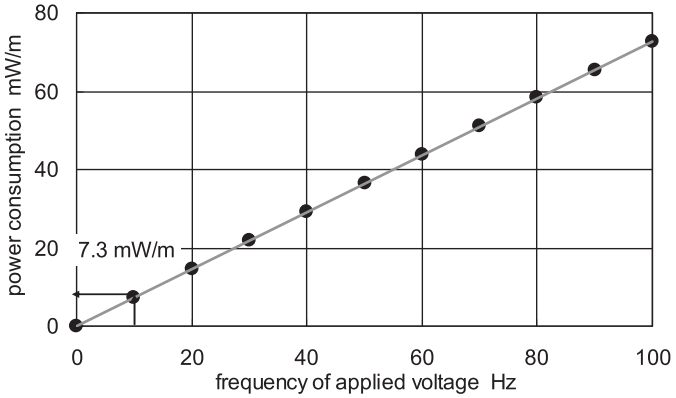

Fig. 6. Power consumption of dust-shielding device (applied voltage: 4 $kV_{p\text{-}p}$); the solid line was obtained by a least-mean-square approximation

J. Aerosp. Eng., 2014, 27(2): 354-358

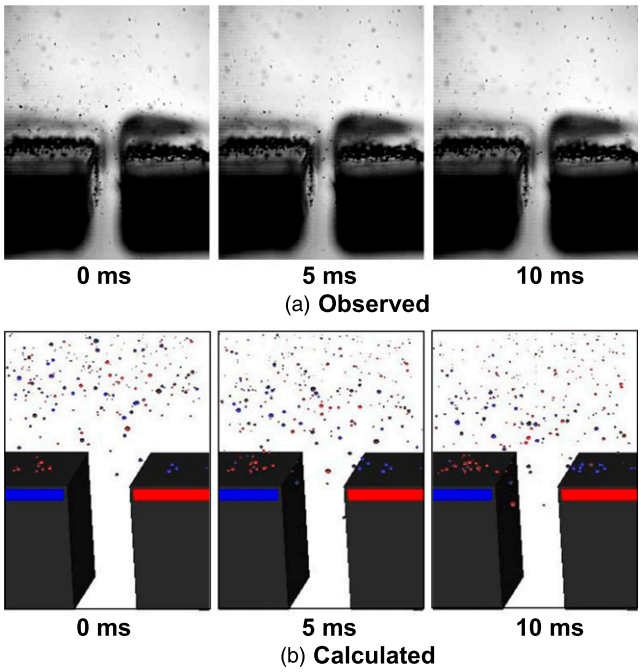

Fig. 7. Observed and calculated motions of particles (2 $kV_{p\text{-}p}$, 10 Hz): (a) observed; (b) calculated

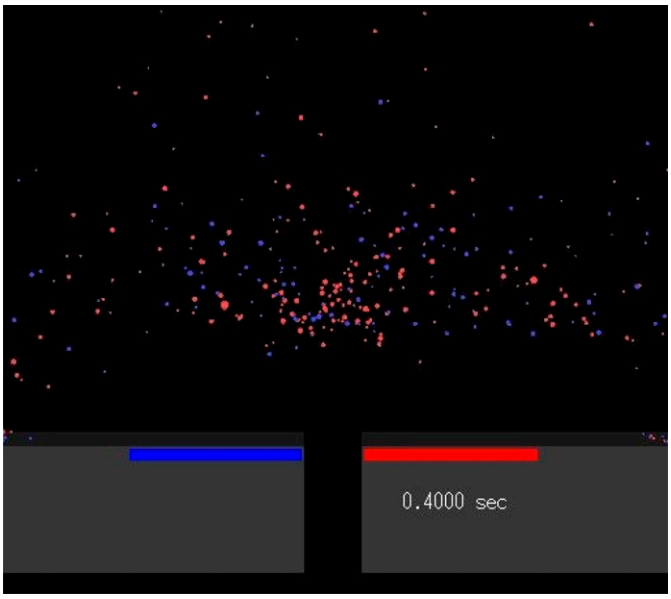

Fig. 8. Calculated motion of particles on the Moon (2 $kV_{p\text{-}p}$, 100 Hz)

E in terms of the Coulomb force consists of the electrostatic field $\mathbf{E}_0$ generated by the power supply and the electrostatic field generated by other charged particles. The field distribution $\mathbf{E}_0$ is calculated by a two-dimensional finite-differential method. The charge q was experimentally determined by measuring it with the Faraday cage as described in the literature (Kawamoto et al. 2006, 2011). The measured charge density was $-0.01 \pm 0.02\,\mu C/g$. The adhesion force was assumed to be proportional to the particle diameter, and the proportional constant was determined experimentally using a centrifugal force (Kawamoto et al. 2011). Eq. (1) was calculated simultaneously for 4,000 to 15,000 particles, depending on the feed rate, using the Runge–Kutta method. For a time-step calculation, the velocities of the particles change owing to particle-particle collisions and particle-device collisions. Linear and angular velocities of the particles after collisions were calculated by a two-body impact equation that included repulsive and frictional effects (Kawamoto et al. 2006). The cyclic boundary condition was imposed in the longitudinal direction to reduce the time required for numerical calculations. The initial condition for the simulation of the particle motion considered particles distributed in an area of length 7 mm, breadth 3 mm, and width 1 mm, and then the particles fell freely from a height of 20 mm to the surface of the device. Diameters and charges of particles were randomly assigned to each particle within the measured data dispersion. These conditions conform to the actual experimental conditions.

Fig. 7 shows the observed and calculated motions of particles in air. Although the dynamic motion of particles cannot be measured from the still images, it was confirmed that the calculated and observed motions are in qualitative agreement.

The calculations were repeated three times under the same conditions except for the random assignment of the initial position and charge. The averages of the calculated shield rates are represented by the open triangle marks in Figs. 4 and 5. It is clearly seen that the calculated results are in reasonable agreement with the observations not only qualitatively but also quantitatively; thus, the present numerical method can be used to predict the performance of the device under conditions that are different from those considered in this study.

Because it is presently impossible to conduct experiments on the Moon, the performance of the system on the Moon was estimated by simulation. The gravity is reduced to g/6 and the air drag is eliminated. The calculated results are also shown in Figs. 4 and 5 using the star symbol. The performance of the system is expected to improve significantly on the Moon.

It is believed that the dust on the Moon is generally charged electrostatically by photoelectric emissions caused by radiation from nearby sources or by electron/ion collisions via sticking or secondary electron emissions (Abbas et al. 2010), and the charge of particles is not discharged in vacuum. Therefore, the charge density of the dust particles on the Moon would be much higher than that measured on the Earth. Fig. 8 shows an example of the calculated results for the highly charged dust particles in the lunar environment. The gravity is reduced to g/6, the air drag is eliminated, and the charge density of the dust is assumed to be $-0.01 \pm 0.1\,\mu C/g$, which is five times that on the Earth. Adjusting the frequency causes the electrostatic field to form a barrier to the dust particles. The dust forms a cloud at altitudes of several millimeters, and virtually no particle will enter the gap. Thus, it is predicted that extremely high shielding performance is achieved on the Moon.

Concluding Remarks

A unique shield system for lunar dust has been developed using electrostatic force to prevent the dust from entering into the bearings and mechanical seals of the equipment used for lunar exploration. The system is suitable for space applications because it is simple and lightweight and also because it does not have moving parts and requires extremely low power.

Although a high performance of the system was demonstrated and numerical calculations predicted further improvement in the low-gravity and vacuum environment of the Moon, it is not possible to achieve complete shielding, as small amounts of dust can still enter into the gaps. However, combination of the proposed shielding device with other devices such as a mechanical brush seal will increase the reliability of the equipment used in long-term manned and unmanned activities on the lunar surface.

J. Aerosp. Eng., 2014, 27(2): 354-358

Acknowledgments

The author extends gratitude to Pei Ye and Yuji Yoshie (Waseda University) for their support in carrying out the research. A part of this study was supported by a Grant-in-Aid for Scientific Research (B) from the Japan Society for the Promotion of Science.

References

Abbas, M. M., Tankosic, D., Craven, P. D., LeClair, A. C., and Spann, J. F. (2010). "Lunar dust grain charging by electron impact: Complex role of secondary electron emissions in space environments." *Astrophys. J.*, 718(2), 795–809.

Calle, C. I., et al. (2010). "Integration of the electrodynamic dust shield on a lunar habitat demonstration unit." *Proc., ESA Annual Meeting on Electrostatics*, Electrostatic Society of America, Rochester, NY, Paper D1.

Delgado, I. R., and Handschuh, M. J. (2010). "Preliminary assessment of seals for dust mitigation of mechanical components for lunar surface systems." *Proc., 40th Aerospace Mechanism Symp.*, NASA Kennedy Space Center, Kennedy Space Center, FL.

Gaier, J. R. (2005). "The effects of lunar dust on EVA systems during the Apollo missions." National Aeronautics and Space Administration (NASA) Glenn Research Center, Cleveland.

Jones, T. B. (1995). *Electromechanics of particles*, Cambridge University Press, New York.

Kanamori, H., Udagawa, S., Yoshida, T., Matsumoto, S., and Takagi, K. (1998). "Properties of lunar soil simulant manufactured in Japan." *Proc, 6th Int. Conf. on Engineering, Construction and Operations in Space,* ASCE, Reston, VA, 462–468.

Kawamoto, H., and Hara, N. (2011). "Electrostatic cleaning system for removing lunar dust adhering to spacesuits." *J. Aerosp. Eng.*, 10.1061/(ASCE)AS.1943-5525.0000084, 442–444.

Kawamoto, H., and Miwa, T. (2011). "Mitigation of lunar dust adhered to mechanical parts of equipment used for lunar exploration." *J. Electrost.*, 69(4), 365–369.

Kawamoto, H., Seki, K., and Kuromiya, N. (2006). "Mechanism on traveling-wave transport of particles." *J. Phys. D Appl. Phys.*, 39(6), 1249–1256.

Kawamoto, H., Uchiyama, M., Cooper, B. L., and McKay, D. S. (2011). "Mitigation of lunar dust on solar panels and optical elements utilizing electrostatic traveling-wave." *J. Electrost.*, 69(4), 370–379.

McKay, D. S., et al. (1991). "The Lunar Regolith." Chapter 7, *Lunar sourcebook*, G. Heiken, D. Vaniman, and B. M. French, eds., Cambridge University Press, Cambridge, U.K., 285–356.

National Aeronautics and Space Administration (NASA) Manned Spacecraft Center. (1970). "Apollo 12 Preliminary Science Report." *Rep. No. NASA SP-235*, Washington, DC.

Suzuki, M., Matsumoto, K., Nishida, S., Wakabayashi, S., and Hoshino, T. (2010). "Experimental study on a brush-type seal in air and in vacuum as a candidate for regolith seal applications." *Proc., 54th Space Sciences and Technology Conf.,* Japan Society for Aeronautical and Space Sciences, Tokyo.

Wagner, S.A. (2006). "The Apollo experience lessons learned for constellation lunar dust management." *Rep. No. TP-2006-213726*, National Aeronautics and Space Administration (NASA), Washington, DC.